

*Supplement of*

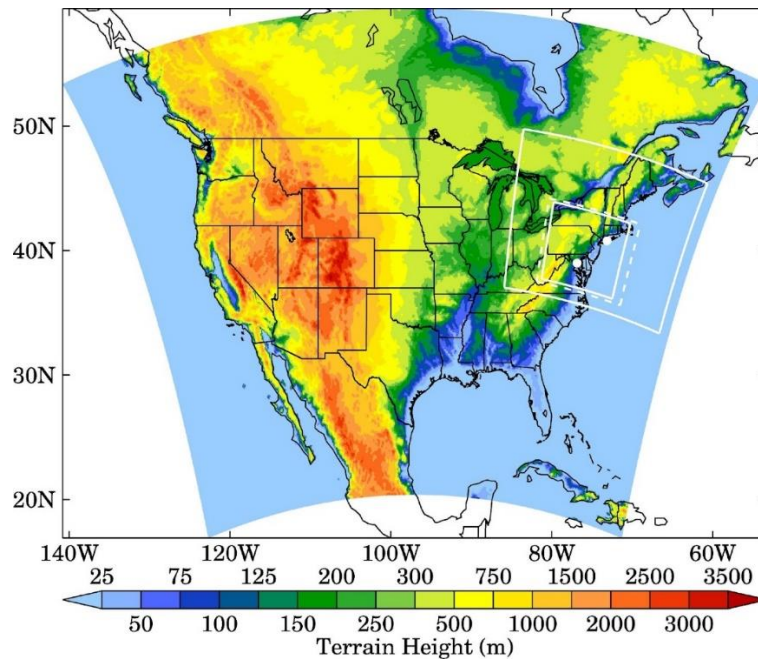
2 **Satellite remote-sensing capability to assess tropospheric column**  
4 **ratios of formaldehyde and nitrogen dioxide: case study during**  
4 **the LISTOS 2018 field campaign**

Matthew S. Johnson et al.

6 *Correspondence to:* Matthew S. Johnson (matthew.s.johnson@nasa.gov)

8 **Table S1. Physical parameterizations used in the WRF model.**

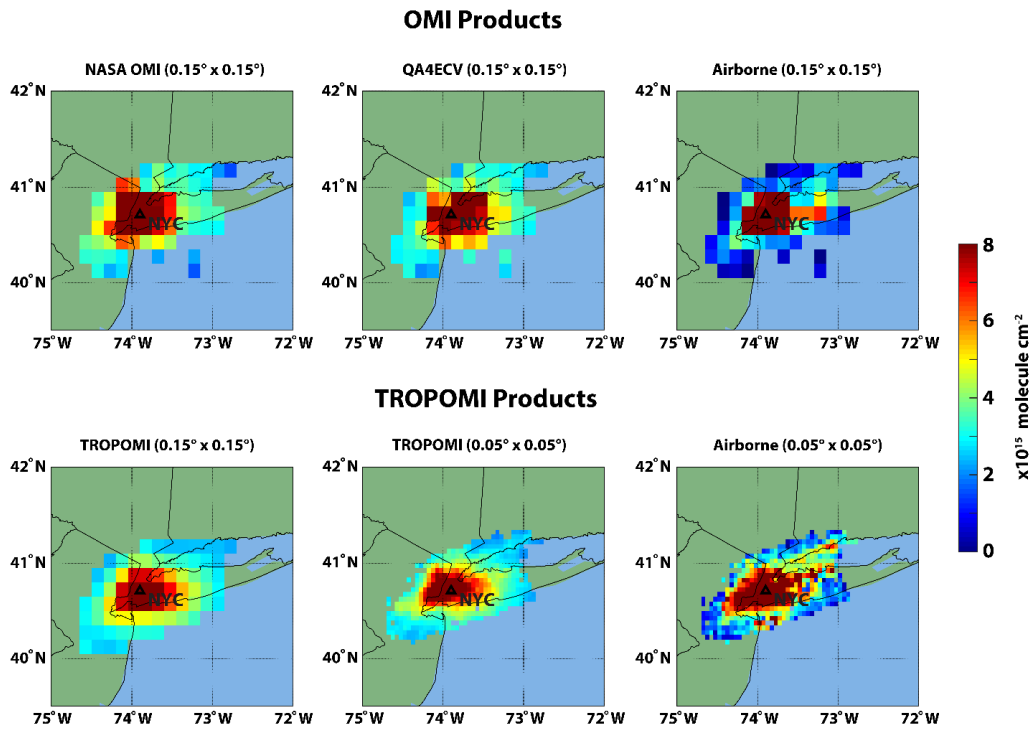
<b>Physical process</b>	<b>Parameterization (Reference)</b>
Long-wave radiation	Rapid Radiative Transfer Model for General Circulation Models (RRTMG) (Iacono et al., 2008)
Short-wave radiation	RRTMG (Iacono et al., 2008)
Microphysics	Morrison double-moment (Morrison et al., 2010)
Cumulus parameterization	Kain–Fritsch version 2 (Kain, 2004)
Land surface model	Pleim–Xiu LSM (Pleim and Xiu, 1995)
Surface Layer	Pleim–Xiu surface layer (Pleim, 2006)
Planetary boundary Layer	ACM2 (Pleim, 2007)



10

12

**Figure S1: WRF-CMAQ modeling domains applied in this study. The white solid lines show the boundaries of the two CMAQ domains while the dotted white lines represent the boundary of the inner WRF domain. Terrain height for the outer WRF domain is also shown. The two white dots mark the regions of focus in the OWLETS-2 and LISTOS 2018 campaigns.**

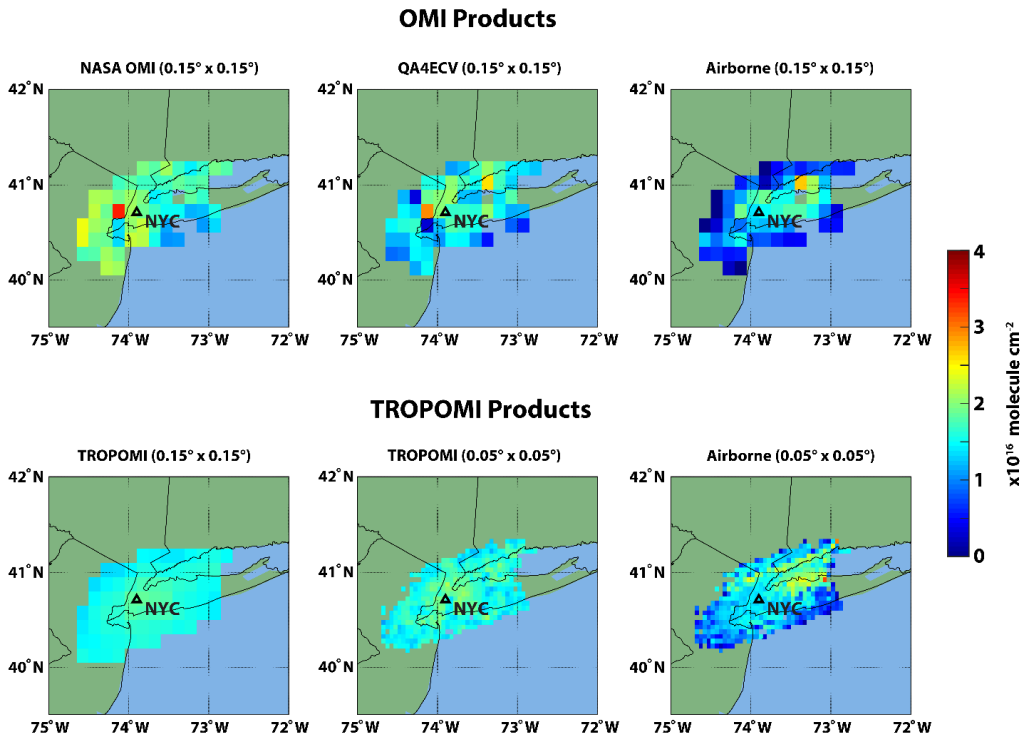


14

16

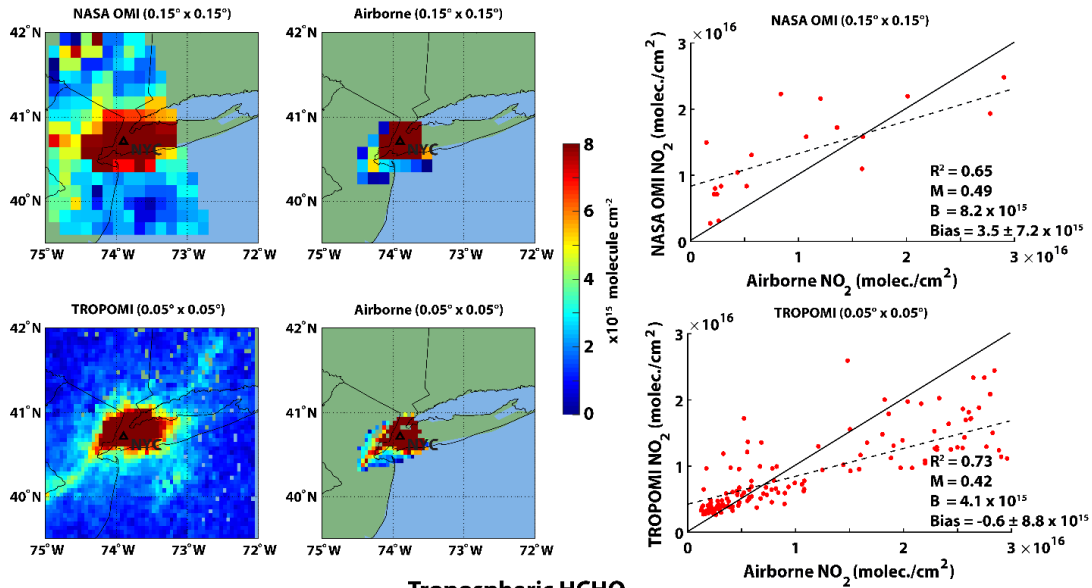
18

Figure S2: NASA OMI, QA4ECV, TROPOMI, and airborne tropospheric column NO<sub>2</sub> retrievals averaged for all flights conducted during the field campaign. All co-located OMI satellite and airborne remote-sensing tropospheric column NO<sub>2</sub> values are averaged at a 0.15° × 0.15° resolution and co-located TROPOMI data are averaged at both 0.05° × 0.05° and 0.15° × 0.15° spatial resolutions. The black triangle indicates the location of the city of NYC.

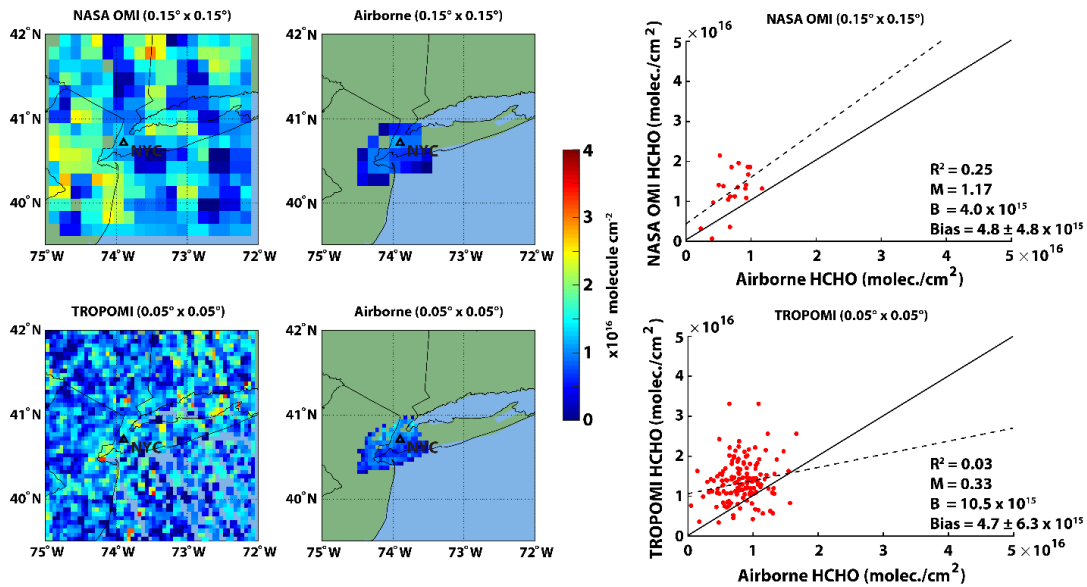


20 **Figure S3: NASA OMI, QA4ECV, TROPOMI, and airborne tropospheric column HCHO retrievals averaged for all flights**  
 22 **conducted during the field campaign. All co-located OMI satellite and airborne remote-sensing tropospheric column HCHO**  
**values are averaged at a  $0.15^\circ \times 0.15^\circ$  resolution and co-located TROPOMI data are averaged at both  $0.05^\circ \times 0.05^\circ$  and**  
 **$0.15^\circ \times 0.15^\circ$  spatial resolutions. The black triangle indicates the location of the city of NYC.**

## Tropospheric NO<sub>2</sub>



## Tropospheric HCHO



24

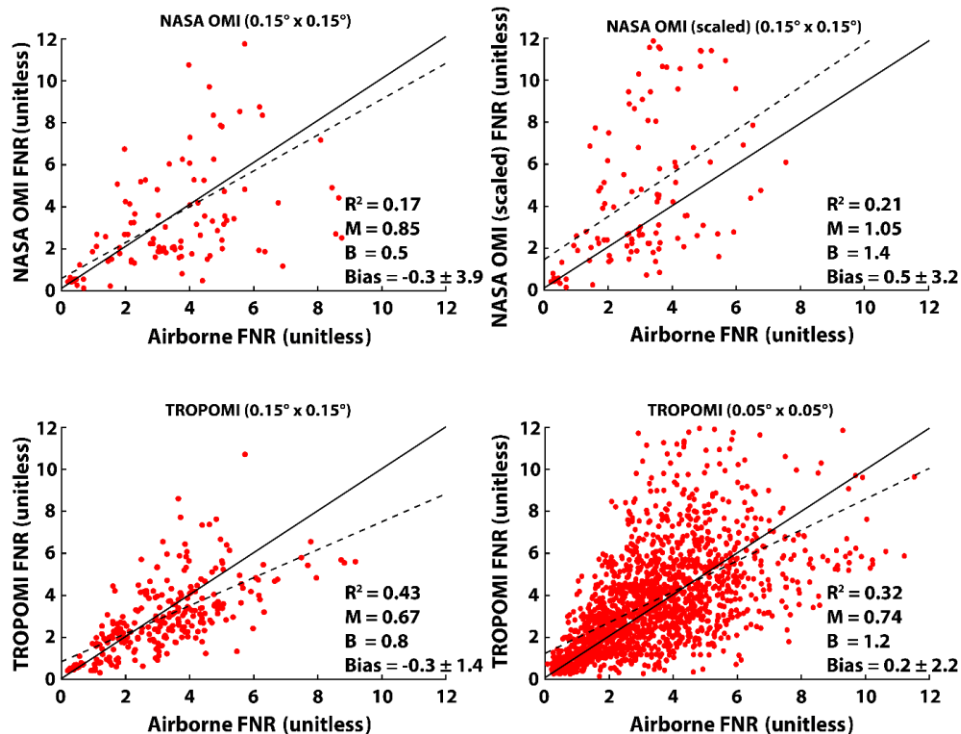
26

28

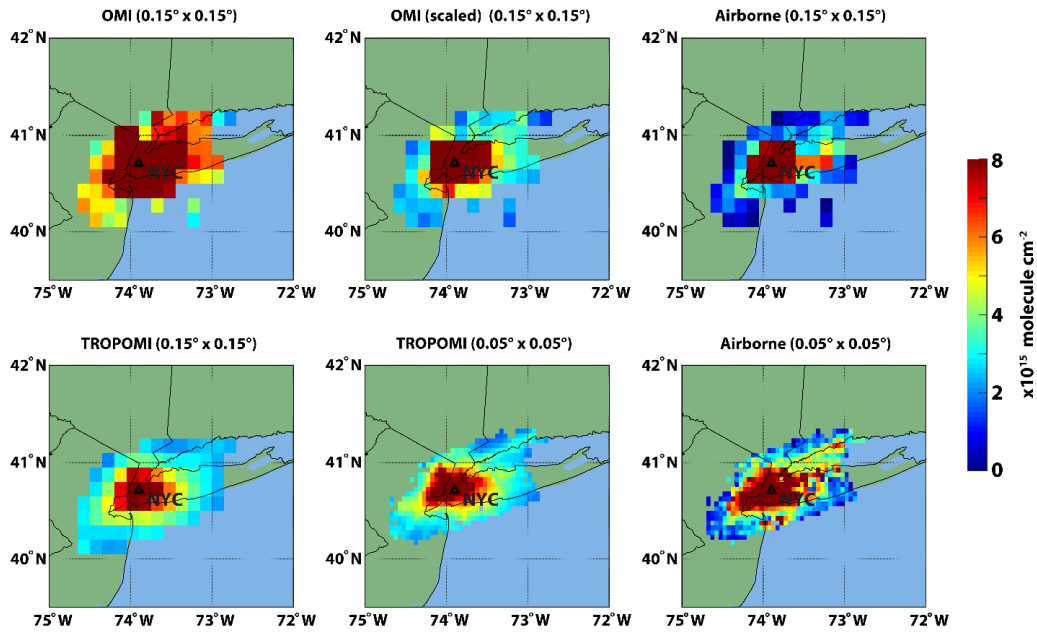
30

32

Figure S4: NASA OMI, TROPOMI, and airborne tropospheric column NO<sub>2</sub> and HCHO retrievals on August 24, 2018. All co-located satellite and airborne remote-sensing tropospheric column NO<sub>2</sub> and HCHO values are averaged at a 0.15° × 0.15° for the OMI intercomparison and 0.05° × 0.05° spatial resolution for TROPOMI. The black triangle indicates the location of the city of NYC. The direct comparison of co-located NASA OMI and TROPOMI NO<sub>2</sub> and HCHO data to airborne observations on this day is shown in the scatter plots (right column). The solid black line shows the 1:1 comparison and the dashed line shows the linear regression fit of the comparison. The figure inset shows the main statistics (coefficient of determination ( $R^2$ ), slope (M), y-intercept (B), and median bias and bias standard deviation) of the comparison of satellite and airborne tropospheric column NO<sub>2</sub> and HCHO data.



34 Figure S5: Scatter plots illustrating the comparison of satellite (NASA OMI and TROPOMI) reprocessed tropospheric  
 36 column FNRs and airborne-retrieved tropospheric FNR (unitless) for each co-located measurement taken during the field  
 38 campaigns. The OMI FNR retrievals calculated with the scaled WRF-CMAQ profiles are identified in the y-axis and titles  
 as “scaled”. The solid black line shows the 1:1 comparison and the dashed line shows the linear regression fit of the  
 comparison. The figure inset shows the main statistics (coefficient of determination ( $R^2$ ), slope (M), y-intercept (B), and  
 median bias and bias standard deviation) of the comparison of satellite and airborne data.

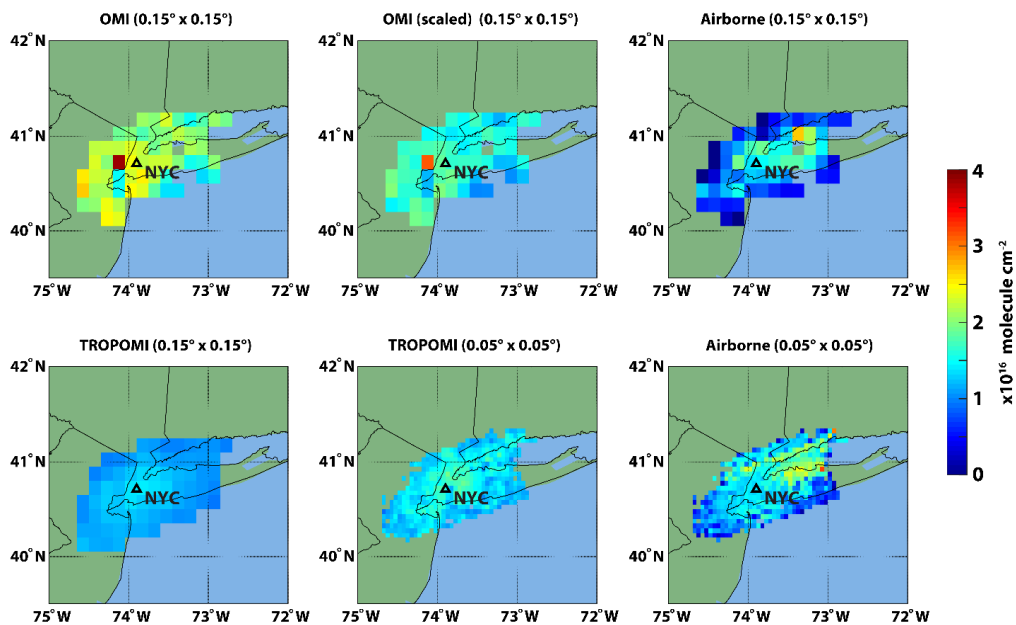


40

42

44

Figure S6: NASA OMI and TROPOMI reprocessed retrievals of tropospheric column NO<sub>2</sub> and airborne observations averaged for all flights conducted during the field campaign. All co-located satellite and airborne remote-sensing tropospheric column NO<sub>2</sub> values are averaged at 0.15° × 0.15° for the OMI intercomparison and 0.05° × 0.05° spatial resolution for TROPOMI. The OMI tropospheric column NO<sub>2</sub> retrievals calculated with the scaled WRF-CMAQ profiles are identified in the titles as “scaled”. The black triangle indicates the location of the city of NYC.

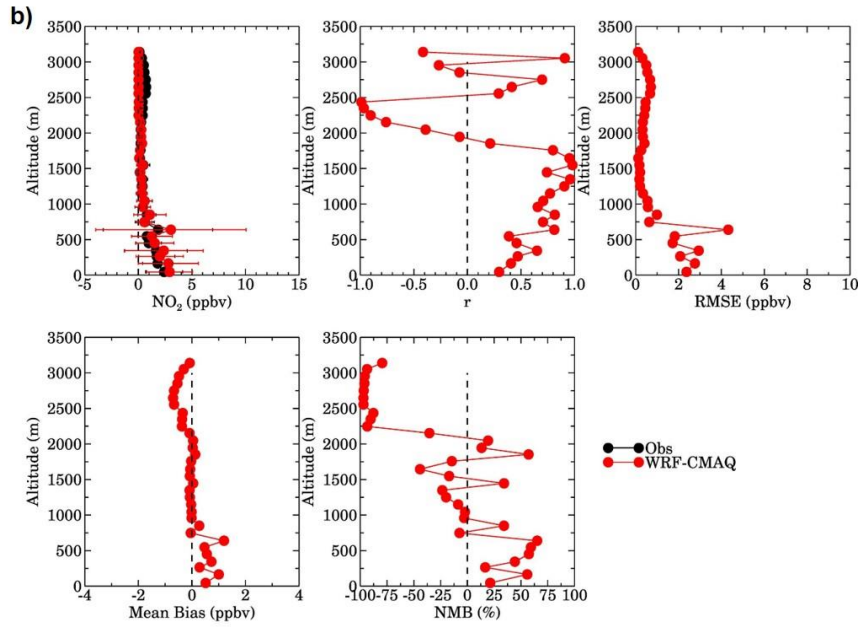
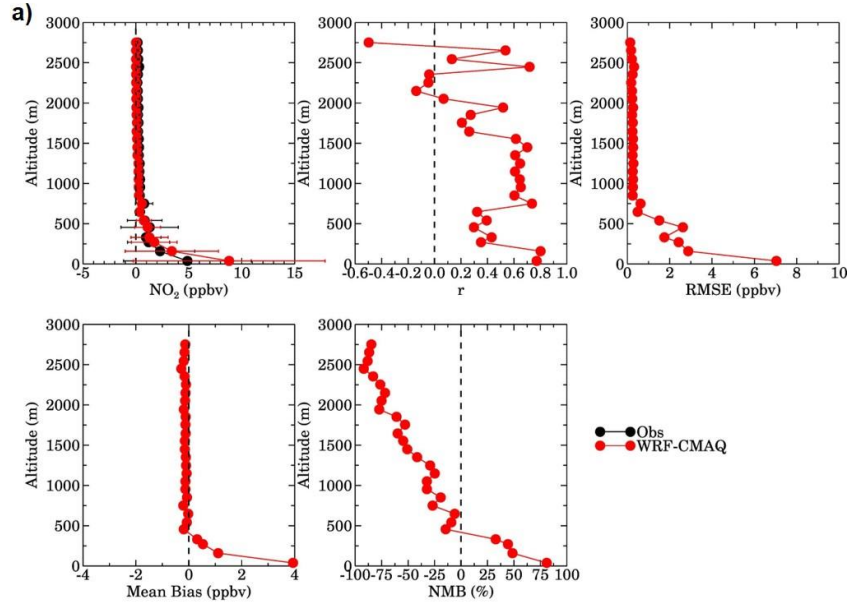


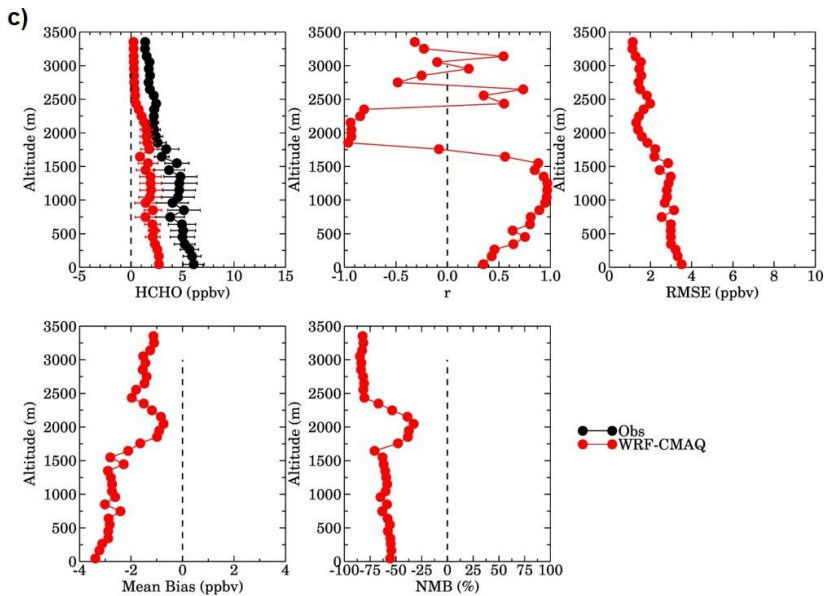
46

48

50

Figure S7: NASA OMI and TROPOMI reprocessed retrievals of tropospheric column HCHO and airborne observations averaged for all flights conducted during the field campaign. All co-located satellite and airborne remote-sensing tropospheric column HCHO values are averaged at  $0.15^\circ \times 0.15^\circ$  for the OMI intercomparison and  $0.05^\circ \times 0.05^\circ$  spatial resolution for TROPOMI. The OMI tropospheric column HCHO retrievals calculated with the scaled WRF-CMAQ profiles are identified in the titles as “scaled”. The black triangle indicates the location of the city of NYC.





54 Figure S8: WRF-CMAQ-predicted concentrations (ppb) of  $\text{NO}_2$  evaluated with airborne observations during a) OWLETS-  
 56 2 and b) LISTOS 2018 and c) WRF-CMAQ-predicted HCHO data during LISTOS 2018. The model (red dots/line) and  
 58 airborne observations (black dots/line) are averaged at 100 m vertical resolution for all measurements during each field  
 campaign. The statistics of the comparison are presented as well.

## References

- 60 Iacono, M. J., Delamere, J. S., Mlawer, E. J., Shephard, M. W., Clough, S. A., and Collins, W. D.: Radiative forcing  
by long-lived greenhouse gases: Calculations with the AER radiative transfer models, *J. Geophys. Res.*, 113,  
62 D13103, doi:10.1029/2008JD009944, 2008.
- Kain, J. S.: The Kain–Fritsch convective parameterization: An update, *J. Appl. Meteor.*, 43, 170–181,  
64 [https://doi.org/10.1175/1520-0450\(2004\)043<0170:TKCPAU>2.0.CO;2](https://doi.org/10.1175/1520-0450(2004)043<0170:TKCPAU>2.0.CO;2), 2004.
- Morrison, H., Thompson, G., and Tatarskii, V.: Impact of Cloud Microphysics on the Development of Trailing  
66 Stratiform Precipitation in a Simulated Squall Line: Comparison of One- and Two-Moment Schemes, *Mon.  
Weather Rev.*, 137, 991–1007, <https://doi.org/10.1175/2008MWR2556.1>, 2009.
- 68 Pleim, J. E. and Xiu, A.: Development and Testing of a Surface Flux and Planetary Boundary Layer Model for  
Application in Mesoscale Models, *J. Appl. Meteorol.*, 34, 16–32, <https://doi.org/10.1175/1520-0450-34.1.16>,  
70 1995.
- Pleim, J. E.: A Simple, Efficient Solution of Flux–Profile Relationships in the Atmospheric Surface Layer, *J. Appl.  
72 Meteorol. Clim.*, 45, 341–347, <https://doi.org/10.1175/JAM2339.1>, 2006.
- Pleim, J. E.: A combined local and nonlocal closure model for the atmospheric boundary layer. Part I: Model  
74 description and testing, *J. Appl. Meteorol. Clim.* 46, 1383-1395, <https://doi.org/10.1175/JAM2539.1>, 2007.